HHS Public Access

Author manuscript

J Comput Assist Tomogr. Author manuscript; available in PMC 2021 January 06.

Published in final edited form as:

J Comput Assist Tomogr. 2016 ; 40(2): 218–224. doi:10.1097/RCT.0000000000000353.

Differentiating Transition Zone Cancers From Benign Prostatic Hyperplasia by Quantitative Multiparametric Magnetic Resonance Imaging

Osama Elbuluk, BS[*], **Naira Muradyan, PhD**[†], **Joanna Shih, PhD**[‡], **Marcelino Bernardo, BS**[*,§], **Sandeep Sankineni, MD**[*], **Maria J. Merino, PhD**[‖], **Bradford J. Wood, MD**[¶], **Peter A. Pinto, MD**[#], **Peter L. Choyke, MD**[*], **Baris Turkbey, MD**[*]

[*]Molecular Imaging Program, National Cancer Institute, National Institutes of Health, Bethesda, MD

[†]iCAD, Inc, Nashua, NH

[‡]Division of Cancer Treatment and Diagnosis, Biometric Research Branch, National Cancer Institute, National Institutes of Health, Bethesda, MD

[§]Imaging Physics, SAIC Frederick, Inc, National Cancer Institute-Frederick, Frederick, MD

[‖]Laboratory of Pathology, National Cancer Institute, National Institutes of Health, Bethesda, MD

[¶]Center for Interventional Oncology, National Cancer Institute, National Institutes of Health, Bethesda, MD.

[#]Urologic Oncology Branch, National Cancer Institute, National Institutes of Health, Bethesda, MD.

Abstract

Objective: The aim of this study was to evaluate the value of quantitative diffusion and perfusion parameters to aid in discriminating between transition zone carcinomas and benign prostatic hyperplasia (BPH).

Materials and Methods: Twenty-four transition zone cancers and BPH nodules were contoured on T2-weighted magnetic resonance imaging (MRI), apparent diffusion coefficient (ADC) maps, and raw dynamic contrast-enhanced (DCE) MRI. Benign prostatic hyperplasia nodules were then stratified into 2 groups based on the presence or absence of a capsule. Apparent diffusion coefficient values, per-voxel K_{trans}, k_{ep}, v_p, and v_e were all compared across all groups.

Results: Average ADCs ($\times 10^{-6}$ mm^2/s) were 1019.22, 1338.11, and 1272.46 for cancer, encapsulated BPH, and nonencapsulated BPH, respectively. Both subgroups of BPH were found to be significantly different than that of cancer ($P < 0.05$). No individual DCE-MRI parameter was significantly different between cancer and either BPH group. The area under the curve for ADC alone was 0.83, and no individual DCE imaging parameter improved the area under the curve of ADC.

Correspondence to: Baris Turkbey, MD, Molecular Imaging Program, National Cancer Institute, 10 Center Dr, MSC 1182, Bldg 10, Room B3B85, Bethesda, MD 20892-1088 (turkbeyi@mail.nih.gov).

Conclusions: Apparent diffusion coefficient may play a role in distinguishing TZ cancers from non-encapsulated BPH nodules that closely resemble cancer.

Keywords

prostate cancer; multiparametric MRI; transition zone; BPH

In 2013, there were an estimated 238, 590 new cases of prostate cancer in men, more than twice that of any other malignancy.[1] Among these cancers, approximately 65% to 70% arise within the peripheral zone (PZ) and 30% to 35% within the transition zone (TZ).[2] Hence, much of the focus on improving diagnostics has been on PZ cancers, where subsequently multiparametric MRI (mp-MRI) has shown great promise with regard to detection and localization.[3-7] On the other hand, TZ cancers have remained relatively elusive and are considered more difficult to accurately diagnose, even with mp-MRI. This largely stems from the presence of benign prostatic hyperplasia (BPH) within the TZ, which can often mask or mimic malignancy. However, TZ cancers can be clinically important and are often missed on conventional transrectal ultrasound–guided biopsy.

The current literature regarding the role of mp-MRI in TZ cancer detection is limited and varies. Transition zone cancers can be distinguished from BPH on T2-weighted (T2W) imaging with fair accuracy using anatomic characteristics such as shape, structure, and growth pattern.[8,9] Features such as homogeneous hypointensity on T2W imaging, ill-defined margins, and lenticular shape have been shown to be specific for TZ cancers.[8,9] Furthermore, the most recent PI-RADS classification has defined T2W imaging as the dominant pulse sequence for identifying TZ cancers.[10] However, visual criteria can be highly subjective, thus decreasing reproducibility. In particular, stromal BPH has been found to very closely resemble TZ cancer on T2W MRI.[11]

Conflicting studies have been published regarding the benefit of diffusion-weighted imaging (DWI) in detecting TZ cancers.[12-17] Multiple studies have shown no added benefit of lower *b* value (<1000 s/mm^2) DWI to T2W MRI at both 1.5 and 3 T.[13-15] On the contrary, it has also been shown that DWI in addition to T2W imaging can improve cancer detection in the TZ across readers with varying expertise.[12] However, these studies only used visual criteria and did not address the potential benefit in high *b*-valued diffusion imaging. In that direction, groups have in fact found that the addition of $b = 2000$ s/mm^2 DWI to T2W provides the highest accuracy in the TZ.[17]

Similarly, DCE MRI has shown contradictory value in detecting TZ cancers across several studies.[11,13,16,18-23] Groups have evaluated quantitative DCE parameters and found no significant difference between BPH nodules and cancer.[18] Yet, others have determined that, when combined with apparent diffusion coefficient (ADC), K_{trans} can improve sensitivity, specifically at low false-positive rates.[11] Thus, the current situation regarding the ability of mp-MRI, specifically functional sequences, to distinguish TZ cancer from BPH remains unsettled.

To improve diagnostics in the TZ, groups have suggested further classifying BPH as stromal or glandular. Stromal BPH appears most like cancer on both T2W imaging and diffusion.

However, many BPH nodules are mixed, and it can be quite difficult to solely define a nodule as entirely stromal or entirely glandular. An easier differentiation may be the presence or absence of a capsule on T2W MRI. The absence of a capsule around a lesion in the TZ has been shown to be highly sensitive for TZ cancers but not specific.[18] Hence, the presence of specifically nonencapsulated BPH greatly increases the difficulty of accurately diagnosing TZ cancers using solely visual information. Thus, we retrospectively evaluated the value of several quantitative mp-MRI parameters in aiding to make the distinction between TZ cancers and BPH by stratifying BPH nodules as encapsulated or nonencapsulated.

MATERIALS AND METHODS

Materials

This is a Health Insurance Portability and Accountability Act-compliant, retrospective, single-institution study, approved by the local institutional review board. Written informed consent was obtained from each patient. Patients were included if, between June 2011 and December 2013, they underwent 3-T mp-MRI with subsequent radical prostatectomy and harbored at least 1 histopathologically confirmed BPH nodule and a TZ cancer at whole-mount histopathology. We identified 24 patients (mean age, 62.45 years; range, 53–71 years; median serum prostate-specific antigen, 8.85 ng/mL; range, 2.74–54.1 ng/mL) who met the inclusion criteria.

MRI Techniques

All MRI studies were performed using a combination of an endorectal coil (BPX-30; Medrad, Pittsburgh, Pa) tuned to 127.8 MHz and a 16-channel cardiac coil (SENSE; Philips Medical Systems, Best, The Netherlands) on a 3-T magnet (Achieva; Philips Medical Systems, Best, The Netherlands) without previous bowel preparation. The endorectal coil was inserted using a semianesthetic gel (Lidocaine; AstraZeneca, Wilmington, Del) while the patient was in the left lateral decubitus position. The balloon surrounding the coil was distended with perfluorocarbon (3 mol/L-Fluorinert; 3M, St Paul, Minn) to a volume of approximately 45 mL to reduce susceptibility artifacts induced by air in the coil's balloon. The MRI protocol included triplanar T2W turbo spin echo, DW MRI (5 *b* values evenly spaced between 0 and 750 s/mm^2), 3-dimensional MR spectroscopy, axial precontrast T1W, axial 3-dimensional T1W fast field echo dynamic contrast-enhanced MRI (DCE MRI) sequences, and their detailed sequence parameters are listed in Table 1. Dynamic contrast-enhanced MRI had 5.6-second temporal resolution, with Magnevist (Bayer, Whippany, NJ) injected after first 3 phases. An additional lower flip angle of 2° dataset was acquired before the DCE sequence for per-voxel T1 relaxation rate calculation to be used for quantitative DCE postprocessing.

Histopathologic Examination

All patients underwent robotic-assisted laparoscopic radical prostatectomy and lymph node dissection as part of their standard of care. The prostatectomy specimen was inked in 4 different colors to provide orientation of the specimen. Then, the prostate gland was fixed in formalin for 24 to 48 hours at room temperature. After fixation, the seminal vesicles were

removed, and the gland was sliced, in the axial orientation of the MRI, from the apex to the base of the gland, at 6-mm intervals while supported inside a customized mold, which was designed for each patient before surgery, using in vivo MRI as previously described.[24] Each slice was sequentially labeled and fixed for a further period of 24 to 48 hours, processed, and paraffin embedded as a whole-mount specimen. The tissue blocks were stained with hematoxylin-eosin for histopathologic evaluation. A surgical pathologist (M.J.M., more than 25 years of experience) who was blinded to the imaging results independently reviewed each stained section. Sections were assessed for the presence of TZ tumors and BPH nodules and then annotated.

MRI Analysis

A research fellow (O.E.) and a genitourinary radiologist (B.T., 7 years of experience in prostate MRI) interpreted all images. They were then analyzed using a commercial DCE-MRI analysis software CADvue (iCAD, Inc, Nashua, NH). The location of TZ cancers mapped on histopathology was determined on axial T2W MR images by identifying anatomic landmarks such as the prostatic urethra and cysts and measuring the distance from those landmarks to the cancer. In addition, the location of the lesion was estimated within the prostate from apex to base, and that served to further help locate the tumor on MRI. Tumors were first contoured on all slices on the T2W MRI on which they were visible. If a patient had multiple cancers within the TZ, only the largest lesion was contoured. Each region of interest was then superimposed on the ADC map and DCE parametric maps using an image registration tool in the DCE-MRI software. The software automatically outputs ADC values as well as mean DCE parameters for the selected region of interest.

Dynamic contrast-enhanced MRI was processed using the extended Tofts model and a group-averaged arterial input function based on the femoral artery signal.[25] Dynamic contrast-enhanced parameter maps included K_{trans} (transfer constant), k_{ep} (rate constant), v_p (fractional plasma volume), and v_e (extravascular extracellular volume fraction) maps from which mean values of each parameter were calculated for all TZ cancers and BPH nodules.

In addition, all TZ cancers were stratified based on their anatomic location. Cancers were defined as either anterior or posterior and either apical, mid, or base of the gland.[10]

Occasionally, small manual adjustments of the maps were needed to compensate for patient motion. In addition, each patient had a histologically confirmed BPH nodule with and/or without a well-circumscribed capsule contoured in the same manner. This nodule was selected by the pathologist without knowledge of the MRI findings. Benign prostatic hyperplasia nodules were relatively well-circumscribed regions with both stromal and glandular components on hematoxylineosin stain. Benign prostatic hyperplasia nodules were stratified by the presence or absence of a well-defined capsule.

Statistical Analysis

We calculated the difference in distribution of each imaging parameter between cancer and both BPH groups by the Wilcoxon test. To account for the intracorrelation of measurements of multiple lesions from the same patient, the bootstrap resampling procedure (number of bootstrap samples, 1000) was used to calculate the standard error (SE) of the Wilcoxon test

statistic, where the sampling unit was patient. *P* values were calculated with the Wald test using the bootstrap SE estimate. Receiver operating characteristic (ROC) and area under the curve (AUC) analyses were performed to assess the overall predictive ability of single as well as multiple imaging parameters. Generalized estimating equations with logit link function and working independence correlation structure were used to find a threshold value in classifying a tumor sample. Each sample was classified as cancer or benign according to whether the logit of the estimated logistic regression model was greater than or less than 0, where logit is defined as $\beta_0 + \beta_1 X$, (β_0, β_1) are the regression coefficients in the logistic regression model, and X is a vector of possibly multidimensional imaging predictors. Sensitivity, specificity, and positive and negative predictive values (PPV and NPV) were then calculated from these imaging-based classifications. In the case of X being multidimensional such as mean ADC and mean K_{trans}, the logit values were used to perform the ROC analysis. The bootstrap resampling procedure (number of bootstrap samples, 1000) was used to calculate the SE and confidence interval of estimated AUC, sensitivity, specificity, PPV, and NPV.

RESULTS

Lesion Location on T2W MRI

Of the 24 BPH nodules contoured, 14 did not have a capsule, and 10 did have a capsule. The locations of the cancers within the TZ are listed in Table 2. Furthermore, 91.6% of cancers were in the anterior portion of the prostate, and 62.5% of all cancers arose within the apex or apical-mid region of the prostate. Only 2 of 24 cancers were found in the posterior region of the TZ, mainly posterior half of the TZ.

Comparison of Each Imaging Parameter Between Cancer and BPH Nodules

Examples of a TZ cancer and a BPH nodule with a capsule are shown in Figure 1, and a BPH nodule without a capsule is shown in Figure 2. The mean values, standard deviations, and 95% confidence intervals of each imaging parameter for all TZ cancers and BPH nodules, with and without a capsule, are listed in Table 3. The mean ADC values were 1019.21×10^{-6} mm^2/s, 1338.11×10^{-6} mm^2/s, and 1272.46×10^{-6} mm^2/s for TZ cancers, BPH with a capsule, and BPH without a capsule, respectively. The results of the comparison of each imaging parameter between nonencapsulated BPH and TZ cancer as well as encapsulated BPH and cancer are shown in Table 4. The Wilcoxon test revealed that the distribution of ADCs differed significantly between TZ cancer and encapsulated BPH ($P < .05$) as well as between TZ cancer and nonencapsulated BPH ($P < 0.0001$). Box plots comparing ADC values between groups are shown in Figure 3. No individual DCE-MRI imaging parameter was found to be statistically different when comparisons were performed between both BPH groups with respect to cancer. Although not statistically significant, the *P* value for k_{ep} showed a trend toward higher values in cancer versus noncapsulated BPH ($P = 0.0596$). Mean k_{ep} values were 1.863, 1.170, and 1.039 min^{-1} for TZ cancer, BPH with capsule, and BPH without capsule, respectively.

ROC Analysis

A threshold ADC value of 1266×10^{-6} mm^2/s was determined to best classify a nodule without a capsule, as BPH or cancer. The sensitivity, specificity, PPV, and NPV were 94%, 64%, 81%, and 82%, respectively. Receiver operating characteristic analysis revealed an AUC of 0.83 (0.73, 0.94) using ADC alone to discriminate cancer from BPH nodules without a capsule (Fig. 4). Multivariate logistic regression was fitted to mean ADC plus any 1 DCE parameter at a time, resulting in 4 multivariate logistic regression models. After accounting for the effect of mean ADC in predicting cancer versus noncapsulated BPH nodules, none of the 4 DCE parameters showed a significant improvement in AUC. Area under the curve values for ADC plus 1 DCE parameter varied from 0.83 to 0.85 versus 0.83 for ADC alone. The corresponding ROC curves are shown in Figure 5.

DISCUSSION

The morphologic features of TZ cancers on preoperative imaging can be difficult to recognize because of the complex architecture of BPH nodules commonly found in the TZ on mp-MRI. Although most BPH nodules are well defined by a pseudocapsule, some BPH nodules can still be ill defined and are difficult to distinguish from TZ cancers. Because BPH nodules rarely harbor prostate cancer if they could be defined as such, the possibility of cancer could be effectively eliminated where BPH nodules can be defined. Numerous studies have shown features such as homogeneous hypointensity, ill-defined margins, lenticular shape, invasion of the anterior fibromuscular stroma, and absence of a capsule on T2W MRI to be consistent with TZ cancers.[8,9] However, these visual characteristics are not only subjective but can commonly overlap with BPH in the TZ. Previous series have cited sensitivities of only 56% to 63% using such visual criteria for detecting TZ cancer.[8] Our study demonstrates that quantitative features derived from DWI may aid in discriminating between TZ cancers and BPH, specifically nodules without a well-defined capsule, a feature closely resembling that of cancer on T2W MRI. Our results show that quantitative ADC values differ significantly between TZ carcinomas and BPH. However, DCE-derived parameters were not as helpful as they did not differ between cancer and noncapsulated or encapsulated BPH. When DCE values were combined with ADC values, there was no improvement in accuracy for differentiation of TZ cancers from BPH nodules.

Unlike PZ cancers, where there is more certain consensus on the value of mp-MRI, the role of mp-MRI in diagnosing TZ cancers remains controversial. Hoeks et al[13] recently evaluated detection and localization accuracy of T2W MRI versus mp-MRI in diagnosing TZ cancers and found no added benefit of DWI and/or DCE. Detection accuracy for T2W MRI alone was 68% versus 66% for mp-MRI ($P = 0.85$). Similarly, AUC values were 0.77 and 0.72 for mp-MRI and T2W MRI alone, respectively ($P > 0.05$). However, this study only used visual criteria. The difficulty in reproducing diagnostic accuracy based on visual criteria alone was highlighted by Jung and colleagues[12] who assessed the incremental value of DWI in addition to T2W MRI for diagnosing TZ cancers. Their findings differed from Hoeks et al, in that DWI was found to increase the AUC from T2W MRI alone for both readers with variable levels of experience ($P = 0.004$ and $P = 0.027$ for each reader, respectively).

Chesnais et al[18] recently proposed that the topological location of nodules could play a significant role in improving TZ cancer diagnosis. Their series demonstrated that the location of nodules in the anteroposterior and superior-inferior direction could be helpful in localizing TZ cancers. This study evaluated 52 consecutive, prostatectomy patients, with 20 histologically confirmed TZ cancers. Among these tumors, all 20 involved the anterior third of the TZ, and 18 of 20 involved the apical third of the TZ. Thus, the posterior and basilar regions of the prostate are relatively less likely to harbor cancers in the TZ, whereas the anterior apical-mid portion of the TZ should be considered a possible “hot spot” for TZ cancer. This agrees with our own observations regarding the location of TZ tumors. These findings in conjunction with the aforementioned visual characteristics of TZ cancers do provide a foundation for improving the diagnostic accuracy of mp-MRI for TZ cancers.

Previous studies have also suggested that quantitative ADC values have some use in identifying TZ cancers. For instance, Oto and colleagues[11] investigated TZ prostate cancers, stromal hyperplasia, and glandular hyperplasia and found mean ADC values to be 1.05×10^{-3} mm^2/s, 1.27×10^{-3} mm^2/s, and 1.73×10^{-3} mm^2/s, respectively. The mean ADC value for TZ cancers in our cohort was 1.019×10 mm^2/s, concordant with previously reported values. The mean ADC value for nonencapsulated BPH was 1.272×10^{-3} mm^2/s, which very closely approximates the mean ADC value of stromal BPH cited by Oto et al. This suggests that most nonencapsulated BPH was likely predominantly stromal with a minor glandular component and explains why TZ cancers are so easily masked by BPH. Because it is impossible to know a priori whether a BPH nodule is stromal or glandular, we chose to select encapsulated and nonencapsulated nodules as a comparison, with the former more likely to be recognized as BPH by observers but the latter often causing confusion with cancer. Benign prostatic hyperplasia nodules defined as glandular hyperplasia by Oto et al were found to have a higher ADC value than any nodules found in our study. Nevertheless, the results are remarkably consistent and suggest that ADC is a robust parameter for distinguishing between BPH and TZ cancer. It should be noted that the choice of *b* values for calculat-ing ADC is often not uniform among studies and this can influence ADC values.[26,27] The lack of consensus across centers regarding MRI protocols presents a formidable barrier for establishing standardized ADC cutoff values. However, it is reassuring that the ADC values from at least 2 independent centers were so consistent.

Dynamic contrast-enhanced MRI parameters were found to be not as useful in distinguishing TZ cancers and BPH. Both BPH and TZ cancers commonly enhance so it would seem difficult to distinguish the 2 simply on the basis of visual enhancement. Furthermore, many BPH nodules are well vascularized, and this likely contributes to the lack of added benefit seen in our study with DCE MRI. Our study showed that DCE parameters varied widely between TZ cancers and were not found to be significantly different than BPH nodules. Van Niekerk and colleagues[28] recently studied TZ cancers and their microvascular density via both immunohistochemistry and microscopy. Their study showed that the microvasculature of TZ cancers was highly heterogeneous, with both hypervascularized and hypovascularized regions. Similarly, TZ cancers showed no consistent increase in microvascular density, area, or perimeter with values that also paralleled those seen in BPH. Others have evaluated TZ tumors and BPH with DCE MRI and corroborated similar results, showing significant overlap between imaging parameters.[29,30] The previously mentioned

study by Oto and colleagues did find that K_{trans} added to the diagnostic accuracy of ADC, especially at lower false positives, which was not the case in our study. Although k_{ep} was not found to be significantly different between TZ cancers and noncapsulated BPH, overall values of BPH tended to be lower than that of cancer. However, almost all TZ cancers enhanced to some degree, whereas some BPH nodules did not enhance. Therefore, the absence of visual enhancement within a lesion favors BPH.

Our study had several limitations. First, the sample size was small. To truly validate this method, it must be applied prospectively to a larger population of patients with a wider range of TZ cancer Gleason grades. Second, the small sample size also diminished the possibility of associating any quantitative MRI metrics with lesion grade. Third, although our method of correlating MRI and histopathology is based on a 3-dimensional printed mold which improves accuracy, nonetheless, there is some inevitable slice misregistration as the slice thickness on MRI is 3 mm and the slice thickness at pathology is 5 μm.

In conclusion, several factors should influence the decision to interpret a TZ lesion as a BPH nodule or as a cancer. We, and others, have shown that cancers tend to occur in “hotspots” within the TZ, particularly anteriorly and apically. Furthermore, quantitative ADC plays an important role in differentiating BPH from TZ cancers. We emphasize that the occurrence of cancer within a well-defined BPH nodule is a rare event, which did not occur in our study. In addition, DCE parameters did not contribute to distinguishing the 2 entities. Thus, diagnosticians should look for cancers between well-defined BPH nodules predominantly in the anterior and apical-mid portions of the gland. Because most nonencapsulated BPH is predominantly stromal, it can be difficult to visually detect, but its ADC values tend to be higher than TZ cancers. Quantitative ADC measurements may add a further layer of confidence to an interpretation. It is in cases where visual criteria are often inconclusive that quantitative mp-MRI is most useful. Our data show that using ADC may improve the diagnostic sensitivity for TZ prostate cancer. Ultimately, larger prospective trials are needed to confirm these initial results and select optimized MRI-derived quantitative parameters for distinguishing between TZ cancers and BPH.

Acknowledgments

Supported by the National Institutes of Health (NIH) Medical Research Scholars Program, a public-private partnership supported jointly by the NIH, and generous contributions to the Foundation for the NIH from Pfizer, Inc; The Doris Duke Charitable Foundation; The Alexandria Real Estate Equities, Inc; Mr and Mrs Joel S. Marcus; and the Howard Hughes Medical Institute as well as other private donors. For a complete list, please visit the Foundation Web site at http://fnih.org/work/education-training-0/medical-research-scholars-program.

REFERENCES

1. Siegel R, Naishadham D, Jemal A. Cancer statistics, 2013. CA Cancer J Clin. 2013;63:11–30. [PubMed: 23335087]
2. McNeal JE, Redwine EA, Freiha FS, et al. Zonal distribution of prostatic adenocarcinoma. Correlation with histologic pattern and direction of spread. Am J Surg Pathol. 1988;12:897–906. [PubMed: 3202246]
3. Hoeks CM, Barentsz JO, Hambrock T, et al. Prostate cancer: multiparametric MR imaging for detection, localization, and staging. Radiology. 2011;261:46–66. [PubMed: 21931141]

4. Ahmed HU, Kirkham A, Arya M, et al. Is it time to consider a role for MRI before prostate biopsy? Nat Rev Clin Oncol. 2009;6:197–206. [PubMed: 19333226]
5. Kirkham AP, Emberton M, Allen C. How good is MRI at detecting and characterising cancer within the prostate? Eur Urol. 2006;50:1163–1174. [PubMed: 16842903]
6. Sciarra A, Barentsz J, Bjartell A, et al. Advances in magnetic resonance imaging: how they are changing the management of prostate cancer. Eur Urol. 2011;59:962–977. [PubMed: 21367519]
7. Turkbey B, Pinto PA, Mani H, et al. Prostate cancer: value of multiparametric MR imaging at 3 T for detection–histopathologic correlation. Radiology. 2010;255:89–99. [PubMed: 20308447]
8. Akin O, Sala E, Moskowitz CS, et al. Transition zone prostate cancers: features, detection, localization, and staging at endorectal MR imaging. Radiology. 2006;239:784–792. [PubMed: 16569788]
9. Li H, Sugimura K, Kaji Y, et al. Conventional MRI capabilities in the diagnosis of prostate cancer in the transition zone. AJR Am J Roentgenol. 186;2006:729–742. [PubMed: 16498100]
10. American College of Radiology. MR prostate imaging reporting and data system version 2.0 Available at: http://www.acr.org/Quality-Safety/Resources/PIRADS/. Accessed February 2015.
11. Oto A, Kayhan A, Jiang Y, et al. Prostate cancer: differentiation of central gland cancer from benign prostatic hyperplasia by using diffusion-weighted and dynamic contrast-enhanced MR imaging. Radiology. 2010;257:715–723. [PubMed: 20843992]
12. Jung SI, Donati OF, Vargas HA, et al. Transition zone prostate cancer: incremental value of diffusion-weighted endorectal MR imaging in tumor detection and assessment of aggressiveness. Radiology. 2013;269:493–503. [PubMed: 23878284]
13. Hoeks CM, Hambrock T, Yakar D, et al. Transition zone prostate cancer: detection and localization with 3-T multiparametric MR imaging. Radiology. 2013;266:207–217. [PubMed: 23143029]
14. Delongchamps NB, Rouanne M, Flam T, et al. Multiparametric magnetic resonance imaging for the detection and localization of prostate cancer: combination of T2-weighted, dynamic contrast-enhanced and diffusion-weighted imaging. BJU Int. 2011;107:1411–1418. [PubMed: 21044250]
15. Haider MA, van der Kwast TH, Tanguay J, et al. Combined T2-weighted and diffusion-weighted MRI for localization of prostate cancer. AJR Am J Roentgenol. 189;2007:323–328. [PubMed: 17646457]
16. Yoshizako T, Wada A, Hayashi T, et al. Usefulness of diffusion-weighted imaging and dynamic contrast-enhanced magnetic resonance imaging in the diagnosis of prostate transition-zone cancer. Acta Radiol. 2008;49:1207–1213. [PubMed: 19031184]
17. Katahira K, Takahara T, Kwee TC, et al. Ultra-high-b-value diffusion-weighted MR imaging for the detection of prostate cancer: evaluation in 201 cases with histopathological correlation. Eur Radiol. 2011;21:188–196. [PubMed: 20640899]
18. Chesnais AL, Niaf E, Bratan F, et al. Differentiation of transitional zone prostate cancer from benign hyperplasia nodules: evaluation of discriminant criteria at multiparametric MRI. Clin Radiol. 2013;68:e323–e330. [PubMed: 23528164]
19. Lemaitre L, Puech P, Poncelet E, et al. Dynamic contrast-enhanced MRI of anterior prostate cancer: morphometric assessment and correlation with radical prostatectomy findings. Eur Radiol. 2009;19:470–480. [PubMed: 18758786]
20. Engelbrecht MR, Huisman HJ, Laheij RJ, et al. Discrimination of prostate cancer from normal peripheral zone and central gland tissue by using dynamic contrast-enhanced MR imaging. Radiology. 2003;229:248–254. [PubMed: 12944607]
21. Sung YS, Kwon HJ, Park BW, et al. Prostate cancer detection on dynamic contrast-enhanced MRI: computer-aided diagnosis versus single perfusion parameter maps. AJR Am J Roentgenol. 2011;197:1122–1129. [PubMed: 22021504]
22. Villers A, Puech P, Mouton D, et al. Dynamic contrast enhanced, pelvic phased array magnetic resonance imaging of localized prostate cancer for predicting tumor volume: correlation with radical prostatectomy findings. J Urol. 2006;176:2432–2437. [PubMed: 17085122]
23. Fütterer JJ, Heijmink SW, Scheenen TW, et al. Prostate cancer localization with dynamic contrast-enhanced MR imaging and proton MR spectroscopic imaging. Radiology. 2006;241:449–458. [PubMed: 16966484]

24. Shah V Pohida T, Turkbey B, et al. A method for correlating in vivo prostate magnetic resonance imaging and histopathology using individualized magnetic resonance-based molds. Rev Sci Instrum. 2009;80:104301. [PubMed: 19895076]

25. Tofts PS. Modeling tracer kinetics in dynamic Gd-DTPA MR imaging. J Magn Reson Imaging. 1997;7:91–101. [PubMed: 9039598]

26. Tan CH, Wang J, Kundra V. Diffusion weighted imaging in prostate cancer. Eur Radiol. 2011;21:593–603. [PubMed: 20936413]

27. Thörmer G, Otto J, Reiss-Zimmermann M, et al. Diagnostic value of ADC in patients with prostate cancer: influence of the choice of b values. Eur Radiol. 2012;22:1820–1828. [PubMed: 22527373]

28. Van Niekerk CG, Witjes JA, Barentsz JO, et al. Microvascularity in transition zone prostate tumors resembles normal prostatic tissue. Prostate. 2013;73:467–475. [PubMed: 22996830]

29. Padhani AR, Gapinski CJ, Macvicar DA, et al. Dynamic contrast enhanced MRI of prostate cancer: correlation with morphology and tumour stage, histological grade and PSA. Clin Radiol. 2000;55:99–109. [PubMed: 10657154]

30. Deering RE, Bigler SA, Brown M, et al. Microvascularity in benign prostatic hyperplasia. Prostate. 1995;26:111–115. [PubMed: 7534916]

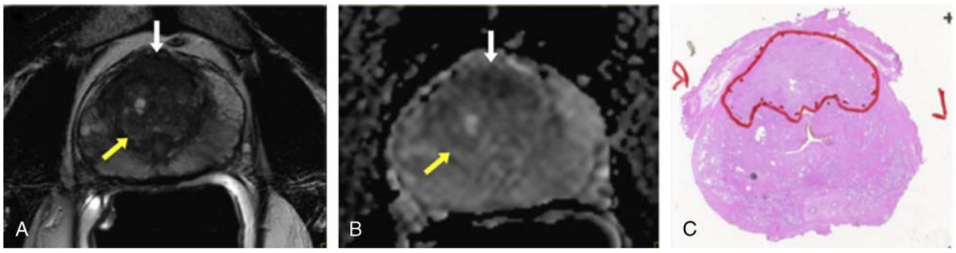

FIGURE 1.

A 53-year-old man with TZ cancer (Gleason score, 3+4) and serum prostate-specific antigen of 15.89 ng/mL. A, Axial T2W MRI demonstrates BPH nodule with a capsule (yellow arrow), which does not resemble the ill-defined low signal intensity midline anterior TZ lesion, which is highly suspicious for cancer (white arrow). B, ADC map showing area of restricted diffusion within the ill-defined anterior TZ lesion suggesting cancer (white arrow) and no restricted diffusion in area of BPH (yellow arrow). C, Surgical specimen confirming anterior TZ cancer (outlined in red).

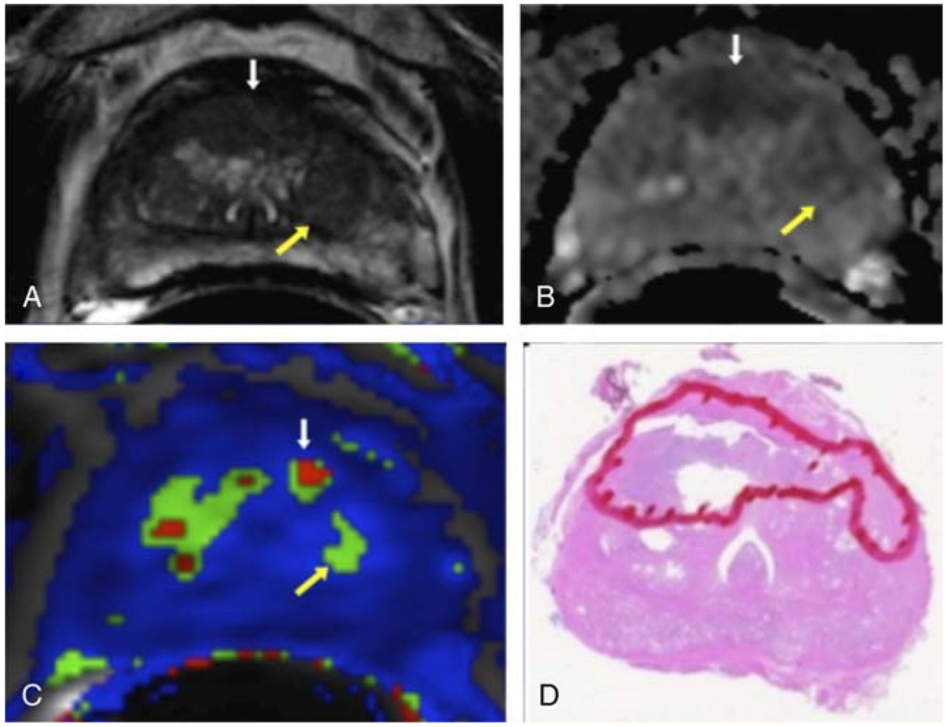

FIGURE 2.

A 59-year-old man with TZ cancer (Gleason score, 4+4) and serum prostate-specific antigen of 12.29 ng/mL. A, Axial T2W MRI demonstrates BPH nodule without a capsule (yellow arrow) and an ill-defined low signal intensity right to the midline anterior TZ lesion suspicious for cancer (white arrow). B, ADC map showing area of restricted diffusion anteriorly (white arrow) suggesting cancer and less restricted diffusion in area of BPH (yellow arrow). C, K_{trans} shows small area of increased K_{trans} values in the tumor (white arrow) and less in the BPH nodule (yellow arrow). D, Surgical specimen confirming anterior TZ cancer (outlined in red).

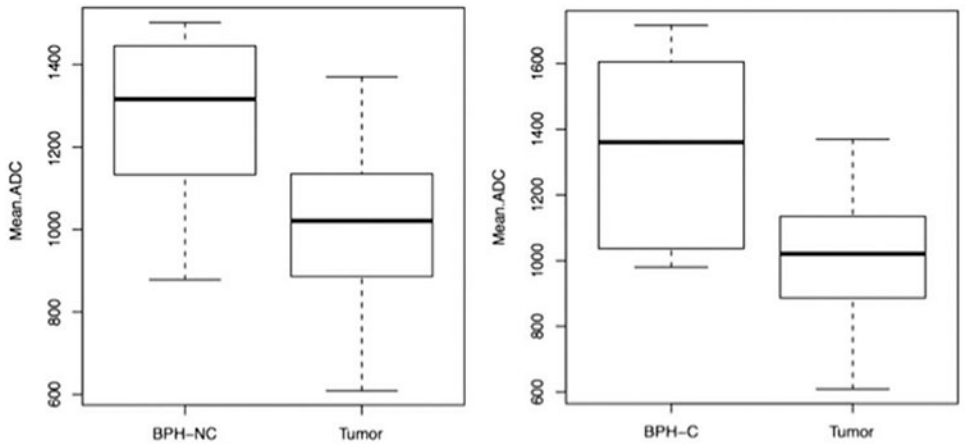

FIGURE 3.

Boxplots comparing ADC values between BPH subgroups and cancer (BPH-NC, BPH noncapsulated; BPH-C, BPH with capsule).

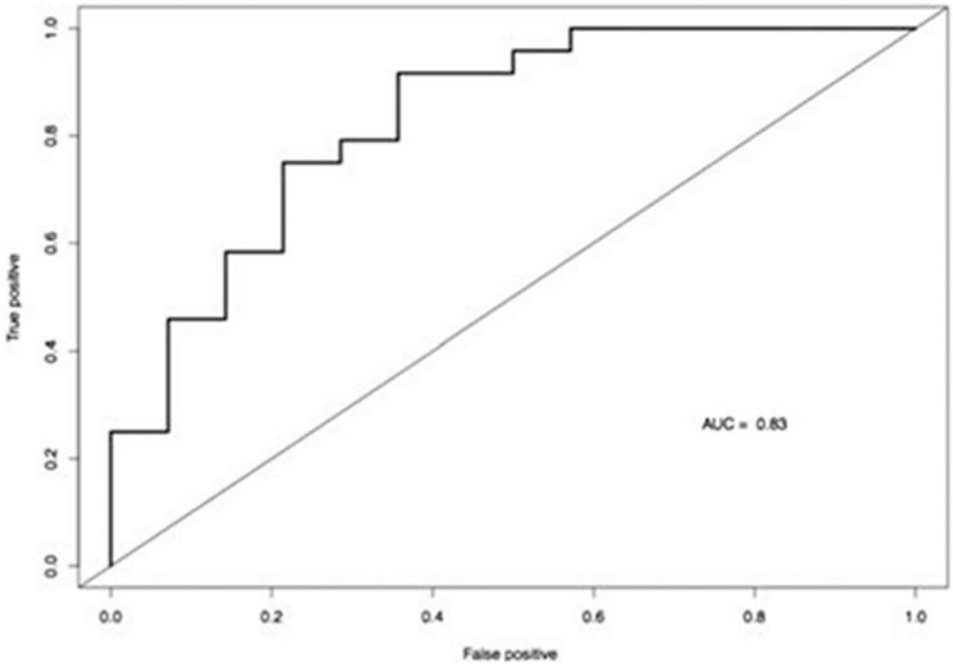

FIGURE 4.
ROC curve for ADC alone; AUC, 0.83.

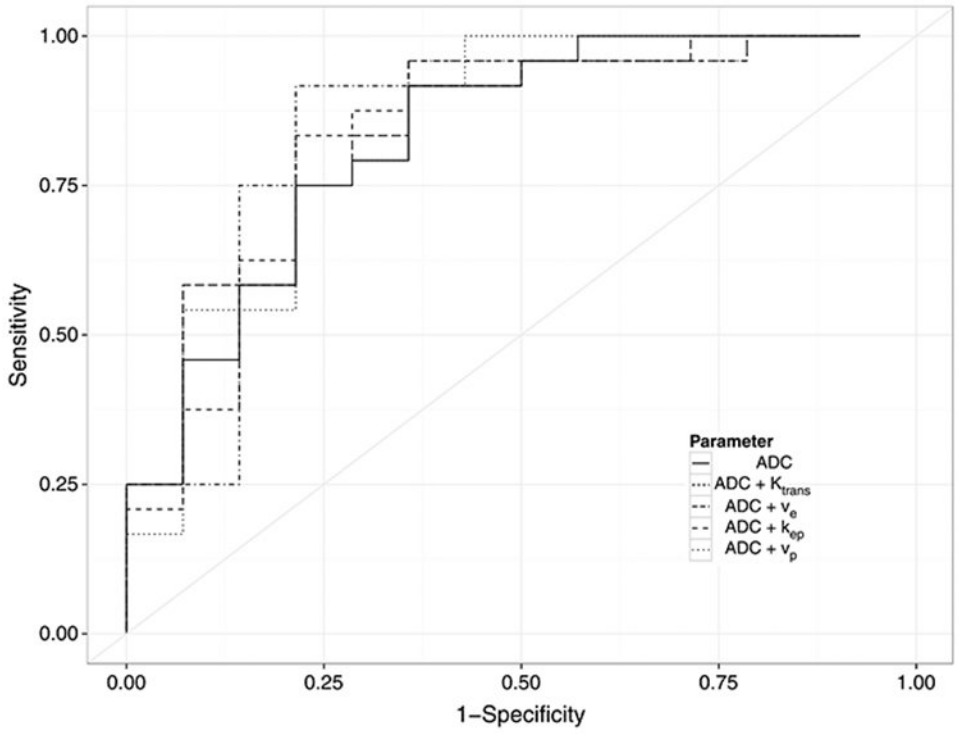

FIGURE 5.
ROC curves for ADC + 1 DCE imaging parameter.

TABLE 1.

MRI Parameters

	T2W MRI	DW MRI	DCE MRI
FOV, mm	140 × 140	140 × 140	262 × 262
Acquisition matrix	304 × 234	112 × 109	188 × 96
TR/TE, ms	4434/120	4986/54	3.7/2.3
Flip angle	90°	90°	8.5°
Slice thickness, no gaps, mm	3.00	3.00	3.00
Image reconstruction matrix, pixels	512 × 512	256 × 256	256 × 256
Reconstruction voxel scanning resolution, mm/pixel	0.27 × 0.27 × 3.00	0.55 × 0.55 × 2.73	1.02 × 1.02 × 3.00
Time for acquisition, min:s	2:48	4:54	5:16

TABLE 2.

Location of TZ Cancers Within the Prostate

Tumor Location	No. Tumors (n = 24)
Anterior	
Apex	7 (29%)
Apical-mid	8 (33%)
Mid	2 (8%)
Mid-base	4 (17%)
Base	1 (4%)
Posterior	
Apex	2 (8%)
Apical-mid	0 (0%)
Mid	0 (0%)
Mid-base	0 (0%)
Base	0 (0%)
Total	24 (100%)

TABLE 3.

The Mean Value, Standard Deviation, and 95% Confidence Interval for Each Imaging Parameter Stratified by Lesion Type

Lesion Type and Parameter	Mean (SD)	95% CI
Cancer		
ADC, $\times 10^{-6}$ mm^2/s	1019.22 (179.65)	667.10–1371.33
K_{trans}, min^{-1}	0.656 (0.43)	−0.182 to 1.494
k_{ep}, min^{-1}	1.863 (1.38)	−0.848 to 4.574
v_p	0.06 (0.03)	−0.001 to 0.121
v_e	0.433 (0.13)	0.174–0.692
BPH with capsule		
ADC, $\times 10^{-6}$ mm^2/s	1338.110 (278.53)	792.2–1884.02
K_{trans}, min^{-1}	0.454 (0.22)	0.16–0.891
k_{ep}, min^{-1}	1.170 (0.59)	0.02–2.32
v_p	0.035 (0.03)	−0.028 to 0.097
v_e	0.435 (0.16)	0.125–0.744
BPH without capsule		
ADC, $\times 10^{-6}$ mm^2/s	1272.460 (199.96)	880.541–1664.387
K_{trans}, min^{-1}	0.495 (0.27)	−0.031 to 1.021
k_{ep}, min^{-1}	1.039 (0.59)	0.119–2.196
v_p	0.049 (0.02)	0.003–0.095
v_e	0.526 (0.20)	0.133–0.919

TABLE 4.

P Values of the Wilcoxon Test Comparing Cancer Versus BPH With Capsule and Cancer Versus BPH Without Capsule

	Mean ADC	Mean K_{trans}	Mean k_{ep}	Mean v_p	Mean v_e
Cancer vs BPH with capsule	0.0016	0.2722	0.2225	0.0784	0.6776
Cancer vs BPH without capsule	<0.0001	0.2188	0.0596	0.3368	0.0803